Isometric embeddings of 2-spheres by embedding flow for applications in numerical relativity

2012 Class. Quantum Grav. 29 155010

(http://iopscience.iop.org/0264-9381/29/15/155010)

IOP Publishing Classical and Quantum Gravity

Class. Quantum Grav. **29** (2012) 155010 (14pp) doi:10.1088/0264-9381/29/15/155010

Isometric embeddings of 2-spheres by embedding flow for applications in numerical relativity*

Michael Jasiulek[1] **and Mikołaj Korzyński**[2]

[1] Max-Planck-Institut für Gravitationsphysik (Albert Einstein Institut), Am Mühlenberg 1, D-14476 Potsdam, Germany
[2] Gravitational Physics, Faculty of Physics, University of Vienna, A-1090 Vienna, Austria

E-mail: michaelj@aei.mpg.de and mikolaj.korzynski@univie.ac.at

Received 29 November 2011, in final form 11 May 2012
Published 3 July 2012
Online at stacks.iop.org/CQG/29/155010

Abstract

We present a numerical method for solving Weyl's embedding problem which consists in finding a global isometric embedding of a positively curved and positive-definite spherical 2-metric into the Euclidean 3-space. The method is based on a construction introduced by Weingarten and was used in Nirenberg's proof of Weyl's conjecture. The target embedding results as the endpoint of an embedding flow in $\mathbf{R}^3$ beginning at the unit sphere's embedding. We employ spectral methods to handle functions on the surface and to solve various (non)linear elliptic PDEs. The code requires no additional input or steering from the operator and its convergence is guaranteed by the Nirenberg arguments. Possible applications in $3+1$ numerical relativity range from quasi-local mass and momentum measures to coarse-graining in inhomogeneous cosmological models.

PACS numbers: 04.25.D−, 02.40.Hw, 02.30.Jr

(Some figures may appear in colour only in the online journal)

1. Introduction

It is a classic result in differential geometry that for every 2-surface of S^2 topology, equipped with a positive-definite metric whose curvature is positive, a global isometric embedding into the Euclidean 3-space can be found. Moreover, the embedding is unique up to the isometries of the Euclidean space which are rigid motions: rotations and translations as well as reflections [1, 2]. This was conjectured by Weyl and later proven by Alexandrov and Pogorelov [3, 4], and independently by Nirenberg [5].

Isometric embeddings into flat space have a wide range of applications in general relativity. For a given isometric embedding in a curved ambient space, they provide a reference surface,

* AEI preprint number: AEI-2011-096, University of Vienna preprint number: UWThPh-2011-42.

thereby fixing the intrinsic geometries. From the difference between the extrinsic geometries, it is possible to define measures of quasi-local mass like the Brown–York and Kijowski–Liu–Yau masses [6–9]. For more examples, see Szabados' review article [10]. Such quasi-local mass measures—not yet applied in (3+1) numerical relativity—could potentially be useful to determine mass and momenta in binary black hole simulations. In addition, the uniqueness of the reference surfaces makes them ideal for visualizing 2-metrics. Another application can be found in 3+1 numerical cosmology where isometric embeddings of S^2 surfaces are the principal step in a method for coarse-graining (averaging) of expansion and shear in inhomogeneous cosmological models proposed by Korzyński in [11, 12].

The isometric embedding equations constitute a three-dimensional (3D) nonlinear, coupled system of PDEs, for which standard numerical methods cannot be applied and analytical solutions are impossible to find. This could be a reason why no practical application to numerical simulations exists. The problem has already been addressed twice: by Nollert and Herold in [13], and by Bondarescu, Alcubierre and Seidel [14]. In the algorithm presented in [13], the 2-surface to be embedded is triangulated and then a corresponding polyhedron in $\mathbf{R}^3$ is constructed, whose edges have a length approximating those of the source triangulation. The method has a serious drawback: multiple polyhedra exist which fulfill the length constraints between neighboring points and most of them converge to unwanted non-regular (non-differentiable) surfaces. For the method in [14], the three unknown embedding functions are expanded into spherical harmonics of maximal degree $l_{\max}$ and the embedding problem is turned into a numerical minimization problem of a $3(l_{\max}+1)^2$-dimensional functional, which vanishes only if the embedding is isometric. This renders the method crucially dependent upon the minimization algorithm used which, among other things, must steer away from the false minima of the functional. The minimization becomes increasingly difficult and computationally costly by increasing the dimensionality of the parameter space.

Our algorithm is based on the continuity method used in Nirenberg's proof and is not affected by the aforementioned problems. Its convergence to the right solution is guaranteed by Nirenberg's theorem. The target embedding emerges as the final surface of an embedding flow beginning with the unit sphere's embedding in $\mathbf{R}^3$. In each step of the flow, the solution of the linearized embedding equation (LEE) allows one to continuously deform the surface from a round unit sphere to the final shape. This procedure requires the conformal factor linking the target and spherical round 2-metric, which we obtain as a steady-state solution of the Ricci flow. However, we note that, unlike the previous two approaches, it is strictly limited to surfaces whose curvature is positive everywhere: even if the isometric embedding exists for a surface with non-positive curvature, the algorithm cannot be applied.

The numerical methods we present in this paper, among others, a pseudo-spectral parabolic evolution scheme to solve the various elliptic PDEs appearing in the problem, could be interesting for other purposes in numerical relativity, too.

The paper is organized as follows: in the next section, we provide the mathematical background, as well as the description of the linearized embedding flow that we use. In the third section, we discuss the technical details of the algorithm and its implementation; in the fourth one, we present the results of a concrete numerical test case. We state the final conclusions in the fifth section and in the appendices, where we also quote relevant but more technical results obtained in this paper.

2. Mathematical background

The Weyl problem can be described as follows: given a 2-surface C of spherical topology, endowed with a positive-definite metric q (target metric), find a sufficiently regular embedding

into the Euclidean space

$$\Phi : C \to \mathbf{R}^3 \tag{1}$$

which preserves the 2-metric q, i.e.

$$q = \Phi^* \delta, \tag{2}$$

where δ is the standard metric on $\mathbf{R}^3$ and Φ^* denotes the standard pullback. In this paper, we assume that the metric and the embedding are smooth.

It is known that the embedding always exists if the metric is sufficiently regular and its curvature is positive everywhere [5, 1]. It is also known to be unique up to the rotations, translation and reflexions in the Euclidean space (see for example [2] for a review of the rigidity results).

Our algorithm to determine Φ is based on the continuity method used in Nirenberg's proof of existence and introduced by Weyl. It consists of three steps which we will now describe briefly, leaving their detailed discussion until the next subsections.

At first we compute the conformal factor relating the target metric to the metric of the round sphere with radius one ${}^0q$ (round metric) which is a steady-state solution of the Ricci flow,

$${}^0q = \mathrm{e}^{-2\sigma}\, q. \tag{3}$$

It is known that the Ricci flow uniformizes the metric [15], i.e. the flow converges to a constant curvature metric $q \to {}^0q$ whereby we obtain σ. In general, the round metric and σ are then given in arbitrary coordinates. This has to be corrected through a transformation, for which the coordinate representation of ${}^0q$ and its embedding Φ_0 into $\mathbf{R}^3$ take a standard well-known form.

Then we construct a one-parameter family of metrics

$${}^tq = \Omega(t, \sigma)^2\, {}^0q, \tag{4}$$

where $\Omega(t, \sigma)$ is a function chosen such that ${}^{t=1}q$ is the target metric and ${}^{t=0}q$ the round metric, which allows one to morph one metric smoothly into the other.

Finally, we perform the embedding flow: beginning at $t = 0$, the known standard embedding Φ_0 of the round metric is deformed in 'small' steps such that the induced metric of the deformed surface at each step matches ${}^tq$ until the target metric is reached. This is accomplished by solving the LEE, which translate a small change of the metric tensor into a small deformation of the embedding functions.

2.1. Ricci flow

In the first step of our method, we have to determine the conformal factor between the target and round sphere metric. In Riemannian 2-manifolds, the Ricci flow reduces to a single equation for the conformal factor

$$\begin{aligned} p(\tau) &= q\, \mathrm{e}^{-2\rho(\tau)} \\ \dot{\rho} &= \mathcal{R}[p(\tau)] - \langle \mathcal{R}[p(\tau)] \rangle, \end{aligned} \tag{5}$$

where $\mathcal{R}[p]$ is the Ricci scalar of the metric p and $\langle \mathcal{R}[p] \rangle$ is its surface average w.r.t. q included to keep the surface area of p bound. $\mathcal{R}[p]$ is related to the Ricci scalar of the target metric in the following way:

$$\mathcal{R}[p] = \mathrm{e}^{2\rho} (\mathcal{R}[q] + 2\, {}^q\Delta \rho), \tag{6}$$

with ${}^q\Delta$ being the Laplacian w.r.t. to q.

The flow converges for large τ to a function $\rho \xrightarrow{\tau\to\infty} \sigma$ for which $\mathrm{e}^{-2\sigma}\, q$ is a round sphere metric (see [16, 15], the latter also in [17]). By a simple rescaling of σ, we can ensure that the sphere has an area of 4π. Now it is possible to construct a family of metrics joining the target and round sphere metric,

$$ {}^{t}q = {}^{0}q\ \Omega(t,\sigma)^2, \tag{7} $$

where $\Omega(t,\sigma)$ should be chosen such that $\mathcal{R}[{}^{t}q]$ is always positive. This is guaranteed for $\Omega(t,\sigma) = \mathrm{e}^{2\sigma t}$. We have also tested a different function to drive the embedding flow $\Omega(t,\sigma) = t(\mathrm{e}^{\sigma} - 1) + 1$, in which the change between consecutive embeddings in the flow, as explained later, is linear in t as well.

2.2. Round metric in standard coordinates

The steady-state solution of the Ricci flow is a round metric ${}^{0}q = \mathrm{e}^{-2\sigma}\, q$ in arbitrary coordinates. In order to realize the isometric embedding of this round metric into the Euclidean space, a transformation to the standard coordinates x^i is required for which the isometric embedding X^i into $\mathbf{R}^3$ takes the well-known form

$$ \begin{aligned} X^1 &= x/r = \sin\theta\ \cos\varphi \\ X^2 &= y/r = \sin\theta\ \sin\varphi \\ X^3 &= z/r = \cos\theta, \end{aligned} \tag{8} $$

unique up to rotations and reflections, where $r = \sqrt{x^2 + y^2 + z^2}$ and (θ, φ) are the spherical coordinates corresponding to x^i. Note that the three functions on the right-hand side of (8) constitute a real, orthogonal basis for the spherical harmonics with $l = 1$. This means that these functions, denoted as n^i, are eigenfunctions of the Laplace operator on the sphere with eigenvalue -2,

$$ \Delta n^i = -2n^i, \quad i = 1, 2, 3. \tag{9} $$

They are also orthogonal and normalized in a sense that

$$ \oint_C n_i\, n_j\, \mathrm{d}A = \frac{4\pi}{3}\, \delta_{ij}\ , \tag{10} $$

where $\mathrm{d}A$ is the area element associated with the round metric. It is easy to check that the opposite is also true: any three orthogonal and properly normalized functions satisfying (9) are related to (8) by a rotation and therefore constitute an isometric embedding of the unit sphere themselves. Equation (9) in turn can be solved numerically even in non-standard coordinates.

2.3. Linearized embedding equation

Consider an S^2 surface D, endowed with a coordinate system θ^A and embedded in $\mathbf{R}^3$ by a mapping described by three functions $X^i(\theta^A)$. The induced metric is given by

$$ q_{AB} = X^i{}_{,A}\, X^j{}_{,B}\, \delta_{ij}. \tag{11} $$

If we deform the embedding by adding a small deviation $\delta X^i(\theta^A)$, the metric changes according to

$$ \delta q_{AB} = 2\, \delta X^i{}_{(,A}\, X^j{}_{,B)}\, \delta_{ij} \tag{12} $$

up to the linear order. Given the metric change δq, one can ask for the compatible deformation vector. Finding δX^i involves solving (12), which is called the LEE. Through a variable transformation, this linear system of three PDEs can be turned into a single elliptic equation

of the second order for Weingarten's 'Verschiebungsfunktion' w, see [18], and two ODEs, see [1, 5] for derivations. Let Y^i denote the deformation vector field that we seek and d_{ij} the metric deformation and let s^i be the outward-pointing normal vector. We decompose Y^i into the normal and tangential part:

$$Y^i = \Upsilon\, s^i + I^i \tag{13}$$

and introduce new variables u_A and w,

$$\begin{aligned} u_A &= s_k\, Y^k{}_{,A}, \\ w &= -\epsilon^{AB}\, D_A I_B. \end{aligned}$$

ϵ^{AB} denotes the area form and D_A is the covariant derivative on the surface. Y^i can be reconstructed from u_A and w via

$$\begin{aligned} \Upsilon_{,A} &= u_A + K_{AB}\, I^B, \\ D_A I_B &= -\tfrac{1}{2} w\, \epsilon_{AB} + \tfrac{1}{2} d_{AB} - \Upsilon\, K_{AB}, \end{aligned} \tag{14}$$

where K_{AB} denotes the extrinsic curvature $K_{AB} = \partial_i s_j\, X^i{}_{,A}\, X^j{}_{,B}$. Equivalently, the equations above can be rewritten as a single equation in the Cartesian coordinates in $\mathbf{R}^3$:

$$Y^i{}_{,j} = \tfrac{1}{2}\left(w\, \epsilon^i{}_{jk}\, s^k + d^i{}_j\right) + s^i\, u_j, \tag{15}$$

with ϵ_{ijk} being the standard antisymmetric symbol, indices raised by δ^{ij}.

On a surface of positive scalar curvature, K_{AB} is positive definite and therefore has an inverse[3]. The variable u_A is then related to the first derivative of w by

$$\begin{aligned} u_A &= -\tfrac{1}{2}\epsilon_{AB}(K^{-1})^{BD}(c_D - w_{,D}), \\ c_D &= -D_A d_{BD}\, \epsilon^{AB}. \end{aligned} \tag{16}$$

The derivation involves differentiating and anti-symmetrizing of (14) and applying the Ricci identity and the Gauss–Codazzi–Mainardi equations, see [1, 5].

Finally, w itself has to satisfy an elliptic equation

$$\mathcal{L} w = \tau \tag{17}$$

obtained as the integrability condition for (16). The elliptic operator $\mathcal{L}$ is defined here as

$$\mathcal{L} w = -D_A((K^{-1})^{AB}\, w_{,B}) - \mathcal{K}\, w, \tag{18}$$

where $\mathcal{K} = K^A{}_A$, and the right-hand side of the equation is

$$\tau = -D_A((K^{-1})^{AB}\, c_B) + K^C{}_A\, d_{BC}\, \epsilon^{AB}. \tag{19}$$

Equation (17) together with (16) and (14) is equivalent to the original LEE.

$\mathcal{L}$ is self-adjoint with the standard scalar product

$$\langle f, g\rangle = \int_C f^*\, g\, \mathrm{d}A[q(t)], \tag{20}$$

and thus has only real eigenvalues. Moreover, for any convex surface it has a three-dimensional kernel spanned by the components of the normal vector $s^1(\theta^A)$, $s^2(\theta^A)$ and $s^3(\theta^A)$ [1]. In particular, in the case of a round sphere, it is possible to show that $\mathcal{L} = -\Delta - 2$.

Since $\mathcal{L}$ has a non-trivial kernel, it is not invertible. Nevertheless, equation (17) has solutions if its right-hand side is orthogonal to the kernel

$$\langle \tau, s^i\rangle = 0 \tag{21}$$

in the sense of (20). It turns out that it is indeed the case if τ is given by (19). The solution w is then unique up to adding a combination of the functions s^i, $i = 1, 2, 3$. Geometrically, this ambiguity corresponds to the possibility of adding a rigid rotation generator to solutions of (12).

[3] The need for global existence of the inverse of K_{AB} is precisely the reason why our method is limited to positively curved metrics.

3. Technical and numerical details

In this section, we explain the numerical and technical details of our implementation. Our approach consists of three main steps: the Ricci flow to link the target and round metric, the $l = 1$ eigenvalue problem of the round metric Laplacian in non-standard coordinates and the embedding flow from the round metric's embedding to the target embedding. For each computational step, we need to conduct a variety of high accuracy numerical operations on spherical surfaces (numerical integration, interpolation, (anti)-differentiation, coordinate inversion, solving elliptic PDEs). For this reason, spectral methods in combination with particular coordinates are the best choice as we explain in the following.

3.1. Coordinate basis, polynomial basis, grid setup

Instead of covering spherical surfaces with 2D coordinate maps, we consider 2-surfaces as being embedded in some (fictitious) ambient Riemannian 3-space (for example, the Euclidian space), endowed with some 3D quasi-Cartesian coordinate system $\{\hat{x}^i\}$, and represent all surface tensors using this exterior coordinate basis. The polar coordinates $(\hat{\theta}, \hat{\phi})$ on the surface are merely used to label the grid points $(\hat{\theta}_i, \hat{\phi}_j)$, $i = 1, \ldots, N_{\hat{\theta}}$, $j = 1, \ldots, 2N_{\hat{\theta}}$. We use a Gauss–Legendre grid structure, the *canonical* grid, on which a surface integral of polynomials of degree $2l_{\max} = 2(N_{\hat{\theta}} - 1)$ can be represented exactly by a finite sum.

Our approach requires various numerical operations on the surface: function evaluations at non-canonical points ('eval'), numerical integration, function inversion ('inv'), differentiation and anti-differentiation ('int'). For this reason, we chose to represent the shape function h and other functions on the surface by an expansion in harmonic polynomials:

$$h = \sum_{lm}^{l_{\max}} {}^{\Phi}[h]^{lm}\, \Phi^{lm} + \mathcal{O}(l_{\max}+1) = \sum_{lm}^{l_{\max}} {}^{Y}[h]^{lm}\, Y^{lm} + \mathcal{O}(l_{\max}+1), \tag{22}$$

where Y^{lm} is the standard othonormalized basis and the other basis is defined by $\Phi^{lm} := \left(\hat{n}^i \mathcal{N}_i^{lm}\right)^l$, where $\hat{n}^i = \hat{x}^i/\hat{r} = (\sin\hat{\theta}\,\cos\hat{\phi}, \sin\hat{\theta}\,\sin\hat{\phi}, \cos\hat{\theta})$ is the radial unit normal. This basis is orthogonal w.r.t. distinct l-eigenspaces. $\mathcal{N}_i$ is a list of constant complex null vectors that span the $2l+1$ harmonics in each eigenspace. The null vectors are chosen as in [19]; then both bases are related by a discrete Fourier transform in each eigenspace.

3.2. Differentiation on the surface

The simple form of the basis $\left(n^i \mathcal{N}_i^{lm}\right)^l$ is practical for evaluation of functions off the grid. In addition, its differentiation[4] is straightforward; for example, the derivative in 3D coordinates takes the form of

$$\partial_i h = \partial_i n^k \sum_{lm} {}^{\Phi}[h]^{lm} \left(n^j \mathcal{N}_j^{lm}\right)^{l-1} l\, \mathcal{N}_k^{lm}. \tag{23}$$

We prescribe 2-surfaces through level set functions G/shape functions h, see figure 1 (left), in some ambient manifold (Σ, γ_{ij}), as is common in numerical simulations of the Einstein

[4] Alternatively, the differentiation of an expansion in Y^{lm}s can be performed by evaluating ∂_i, $\partial_{ij} Y^{lm}$ from ∂_i, $\partial_{ij}\Phi^{lm}$. It is practical to tabulate the ∂_i, $\partial_{ij} Y^{lm}$ at the beginning.

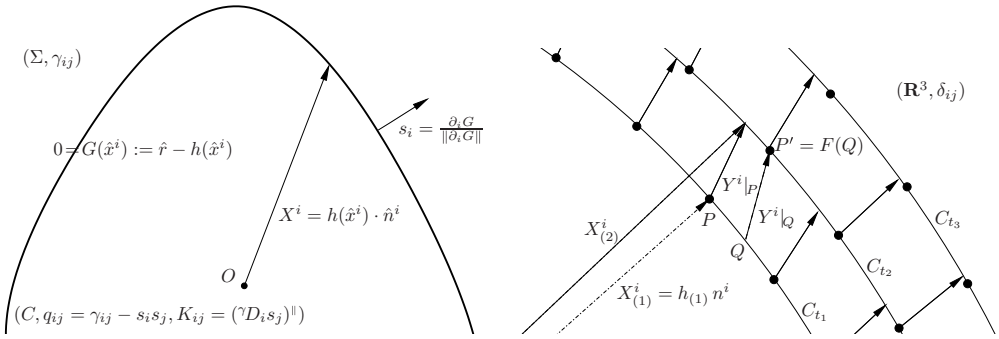

Figure 1. Left: the level surface (C, q_{ij}) given by $G(\hat{x}^i) = \hat{r} - h(\hat{x}^i)$ at $G = 0$ and the induced metric q_{ij} in the Riemanian manifold (Σ, γ_{ij}). Right: embedding flow at $t = t_1, t_2, t_3$ in the Euclidean space. The shift vector field Y^i at each step induces a new embedding $F : X^i_{(1)} \mapsto X^i_{(2)} = X^i_{(1)} + Y^i$ that is in general located off the canonical grid (dots).

equation in (3+1) dimensions. If a shape function h is given, the computational steps to calculate curvature tensors on the surface are as follows:

$$\begin{aligned} h \;\to\; [h]^{lm} \;\to\; \partial_i h,\, \partial_{ij} h \;\to\; s_i, q_{ij}, K_{ij} \;\to\; \mathcal{R}, K^{(\text{-}1)}_{ij} \\ \partial_{ijk} h \;\to\; \partial_i K_{jk} \;\to\; \partial_i K^{(\text{-}1)}_{jk}, \end{aligned} \tag{24}$$

where the expressions in bold are only necessary for solving the LEE.

The computation of curvature tensors on the surface requires the covariant derivative ${}^{q}D_i \chi_j$ w.r.t. q of a tensor χ_i, which might has a normal component $\chi_s \neq 0$, as for example $\partial_i h$,

$${}^{q}D_i \chi_j = ({}^{\gamma}D_i \chi_j)^{\parallel} - K_{ij} \chi_s, \tag{25}$$

which is not simply the tangential part of the ambient derivative $({}^{\gamma}D_i \chi_j)^{\parallel}$. As a consequence, the Laplacian of a function ψ on C is calculated by

$${}^{q}\Delta \psi = q^{ij} \partial_{ij} \psi - {}^{\gamma}\Gamma^i \partial_i \psi - \mathcal{K}\, \partial_s \psi, \tag{26}$$

where ${}^{\gamma}\Gamma^i = {}^{\gamma}\Gamma^i_{jk}\, q^{jk}$ and ${}^{\gamma}\Gamma^i_{jk}$ are the Christoffel symbols of γ.

3.3. Parabolic flow relaxation method

The elliptic PDEs of the type $\mathcal{L}(u) - V(u) = 0$ appearing in our approach are solved by considering the associated parabolic flow equation[5]

$$\dot{u} = \mathcal{L}(u) - V(u) \quad \xrightarrow{-\langle \text{rhs} \rangle} \quad \dot{u} = \{\mathcal{L}(u) - V(u)\}^{/l=0}, \tag{27}$$

where $\dot{u}$ is the time derivative of u and $\{\bullet\}^{/l=0} := \bullet - \langle \bullet \rangle$ removes a function's surface average ($l = 0$ mode). For the linear elliptic operators $\mathcal{L}$ with a non-positive spectrum, except $l = 0$, arbitrary initial data evolve to a steady-state solution (at $\dot{u},\ \ddot{u},\ \ldots = 0$) of the parabolic PDE which is automatically a solution to the elliptic equation. The Ricci flow is a parabolic PDE with a nonlinear elliptic part. The existence of its steady states and convergence to them are known [16, 15].

[5] In principle, the spectral decomposition of functions on the surface would allow us to turn nonlinear/linear elliptic PDEs into algebraic/linear systems of equations to be solved with Newton–Raphson's/splitting (relaxation) methods which are numerically more efficient but more stringent with regard to the initial guess and the conditioning of involved matrices. The parabolic flow relaxation method on the other hand covers nonlinear/linear elliptic PDEs and is more robust. Moreover, efficiency is not a concern for the 2D PDEs we deal with.

The parabolic PDEs we deal with are solved by means of a pseudo-spectral scheme, where we use the method of lines, second- or fourth-order Runge–Kutta (RK2, RK4) and spectral spatial differencing, see equation (23), until $|\dot{u}|$ falls below machine/spectral precision (exponentially). Since we are not interested in the details of the solution during the relaxation period, but in a quick fall-off, we pick a coarse time-step Δt and RK2 (Heun), where we take the CFL condition of the heat equation with explicit Euler $\Delta t < \nu(\Delta x)^2$, $\nu = 0.25$ as an orientation.

The algebraic operations to compute the rhs produce an aliasing error. Therefore, we filter modes $> l_{\max}$ form the rhs.

3.4. Computational steps: Ricci flow, EVP, LEE

The computational steps of the main component 'Ricci flow' of our implementation are the following. A shape function $h(\hat{x})$ and an ambient geometry, see figure 1 (left), are required as input,

$$h(\hat{x}) \quad \to \quad \text{equation (24)} \quad \to \quad \text{evolve: } \dot{\sigma} = \{\mathcal{R}[\mathrm{e}^{2\sigma} q]\}^{/l=0} \quad \to \quad \sigma(\hat{x}), {}^0q(\hat{x})_{ij},$$

where $\mathcal{R}[\mathrm{e}^{2\sigma} q] = \mathrm{e}^{2\sigma}(\mathcal{R}[q] + 2\,{}^q\Delta\sigma)$ and ${}^q\Delta\sigma$ is computed as in equation (26). The spherical round metric ${}^0q_{ij} = \mathrm{e}^{-2\sigma} q_{ij}$ with $\mathcal{R}[{}^0q] \equiv 2$ is the steady-state solution of the Ricci flow. It is given in non-standard coordinates in which its Laplacian takes the form ${}^0\Delta\bullet = \mathrm{e}^{2\sigma}\,{}^q\Delta\bullet$. As a standard coordinate basis, we take the three orthonormalized $l = 1$ eigenfunctions n^j of ${}^0\Delta$, see equation (8),

$$\sigma(\hat{x}) \quad \to \quad \text{evolve: } \dot{n}^i = \{{}^0\Delta n^i + 2n^i\}^{/l=0} \quad \to \quad n^j(\hat{x}) \xrightarrow{\text{inv}} \hat{n}^i(x) \xrightarrow{\text{eval}} \sigma(x)$$

in which ${}^0q$ takes the well-known simple form ${}^0q_{ij} = \delta_{ij} - n_i n_j$. Identifying x^i with Cartesian coordinates in $\mathbf{R}^3$ maps ${}^0q_{ij}$, σ to the Euclidean space where the embedding flow is performed, see figure 1 (right). We construct a family of metrics ${}^tq_{ij} = \Omega(t,\sigma)^2 \cdot {}^0q_{ij}$ such that ${}^{t=0}q \equiv {}^0q$ and ${}^{t=1}q \equiv q$ with $\mathcal{R}[{}^tq] > 0$ and divide the time interval into N steps, i.e. $t = 0, t_1, t_2, \ldots, t_N$[6] whereby we slowly deform ${}^tq$ into the target metric such that the difference

$$ {}^{(n)}d_{ij} := q(t_{n+1})_{ij} - {}^{(n)}q_{ij} \tag{28}$$

is small, where ${}^{(n)}q_{ij}$ is the induced metric w.r.t. $h_{(n)}$, see figure 1 (left), at the nth step. We initialize the flow with the shape function $h_{(0)} = 1$ corresponding to the standard embedding of the unit sphere. At every step, we compute

$$\begin{aligned} h_{(n)} &\to \text{equation (24)} \quad \to \quad \text{compute: } {}^{(n)}d_{ij} \quad \to \quad \text{evolve: } \dot{w} = \{(\mathcal{L}(w) - \tau)/\mathcal{K}\}^* \\ &\to w \xrightarrow{\text{int}} Y^i|_P \quad \to \quad n^i_{(n+1)}(x|_P) \xrightarrow{\text{inv}} n^i(x_{(n+1)}|_{P'}) \xrightarrow{\text{eval}} (Y^i, \partial_j Y^i, \sigma, q_{ij})|_Q \\ &\to (h_{(n+1)}, q_{ij})|_{P'}, \end{aligned}$$

where $*$ denotes projecting out the lowest eigenvalue of $\mathcal{L}$ (see appendix A). Complications arise from the fact that the new embedding induced by Y^i is shifting the points off the canonical grid. Moreover, the target metric (${}^0q$ and σ) has to be transported under the mapping $X^i_{(n+1)} = X^i_{(n)} + Y^i$ from one surface to the other,

$$q_{ij}|_{P'} = \frac{\partial X^k_{(n)}}{\partial X^i_{(n+1)}} \frac{\partial X^l_{(n)}}{\partial X^j_{(n+1)}} q_{kl}|_Q. \tag{29}$$

[6] The number of steps and the values t_n are arbitrary and depend on how far q is off the round metric, usually $3 < N < 7$.

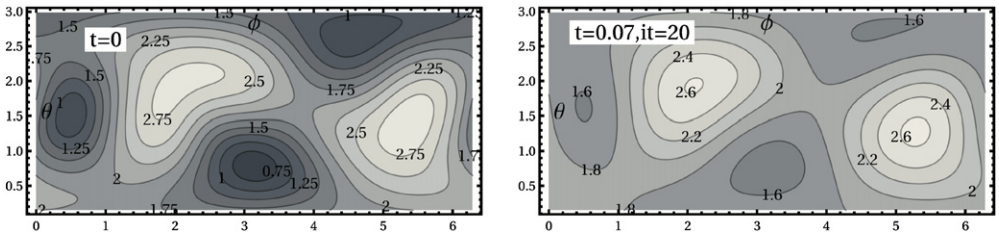

Figure 2. (θ, ϕ)-contour plots of the scalar curvature $\mathcal{R}[{}^{t}q]$ in relaxation flow at $t = 0$ and $t = 0.07$.

After N equi-distant steps $h_{(N)}$, difference (28) between the target metric and the induced metric w.r.t. $h_{(N)}$ is of the order $N \cdot \mathcal{O}(d^2)$. But this solution can be refined by recursively applying[7] the above computational steps with ${}^{t=1}q_{ij}$ fixed in equation (28) whereby d_{ij} converges to zero exponentially.

4. Numerical test case

In this section, we apply our procedure to a numerical test case, where we prescribe a test shape function in the Euclidean space given by the function below. We solve the embedding problem numerically and compare the original embedding with the resulting one. More specifically, we compute the induced 2-metric, perform the Ricci flow to the round sphere, solve the EV problem and perform the embedding flow from the round sphere to the target shape, solving the LEE at each step.

As a test case we pick a cigar-shaped function (for illustration purposes) and add a randomized non-polynomial part

$$h = c_1\big(1 + c_2\,\mathrm{Re}\big[\big(\mathcal{N}_1^j n_j\big)\big]^2 + \sqrt{1 + c_3\,\mathrm{Re}\big[\big(\mathcal{N}_2^j n_j\big)^2 + \big(\mathcal{N}_3^j n_j\big)^3\big]}\big),$$

where $c_{1,2,3} = 0.458,\ 0.5,\ 0.15$ (for which the area $A \approx 1$ and $\mathcal{R} > 0$, $\mathcal{K} > 0$) and $\mathcal{N}_{1,2,3}$[8] are three randomly oriented null vectors. Then all lm modes are populated in a somewhat random manner. The surface defined by this shape function has the following area and central n-moments of the curvature ${}^{n}\sqrt{\mu_n(\bar{\mathcal{R}})}$:

$$A/4\pi = 0.999\,285, \qquad \sqrt[2]{\mu_2(\bar{\mathcal{R}})} = 0.280\,044,$$
$$\sqrt[3]{\mu_3(\bar{\mathcal{R}})} = 0.197\,685, \qquad \sqrt[4]{\mu_4(\bar{\mathcal{R}})} = 0.342\,832,$$

where

$$\mu_n(\bullet) := \langle(\langle\bullet\rangle - \bullet)^n\rangle,$$

and $\bar{\mathcal{R}} = c\,\mathcal{R}$ with $\langle\bar{\mathcal{R}}\rangle = 1$. As shown in figure 2 (left), the scalar curvature significantly differs from that of a round sphere initially, where $\sigma = 0$ is set, but smoothes out toward $\mathcal{R} \approx 2$ in the Ricci flow (right), where we employ the relaxation method as explained in the last section. The fall-off is exponential, see figure 3 (left), until it reaches a plateau of truncation error which converges to zero by increasing the spherical resolution. The second-order scheme is computationally more efficient, since the parabolic flow is stable up to $\nu = 0.11$ for RK2-Heun and up to $\nu = 0.16$ for RK4[9] (measured for $N_\theta = 16$, $\mathrm{d}x = 0.186$).

[7] If necessary this refinement process can be applied at any intermediate time t_n, such that the embedding flow does not move too far off the conformal metric flow.

[8] $\mathrm{Re}[\mathcal{N}_{1,2,3}] = 1/\sqrt{434}(-9, 17, -8)$, $1/\sqrt{3786}(-1, -43, 44)$, $1/\sqrt{78}(7, -2, -5)$ and $\mathrm{Im}[\mathcal{N}_{1,2,3}] = -1/\sqrt{3}(1, 1, 1)$.

[9] On the same surface solving the heat equation, we obtained $\nu = 0.20$ RH2-Heun, $\nu = 0.28$ RH4.

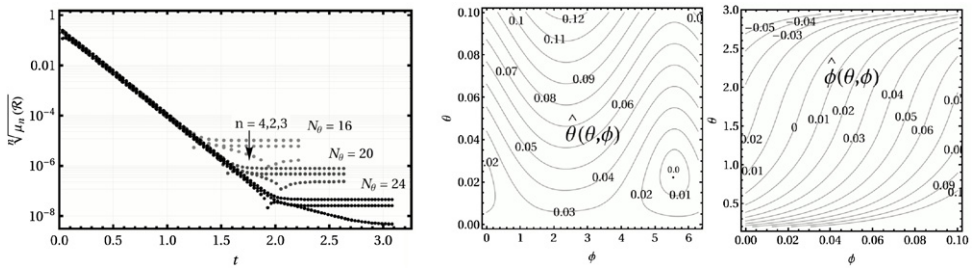

Figure 3. Left: exponential fall-off of $\sqrt[n]{\mu_n(\tilde{\mathcal{R}})}$ for $n = 2, 3, 4$ at three different resolutions $N_\theta = 16, 20, 24$. Right: 'old' $(\hat{\theta}, \hat{\phi})$-coordinates given in the new (θ, ϕ)-coordinates.

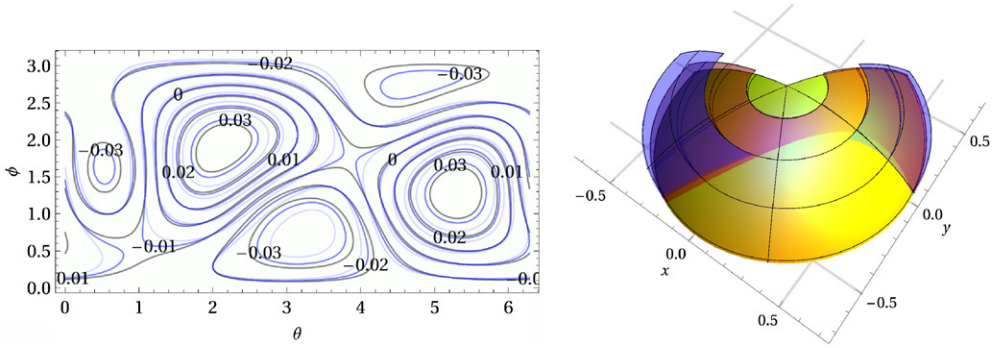

Figure 4. Left: contours of difference $h_{(n+1)} - h_{(n)}$ between consecutive shape functions $h_{(n)}$ for $n = 1, 2, 3$ in embedding flow (black 3−2, blue 2−1, light blue 1−0). Right: embedding flow at $t_{n=0,2,3} = 0.0, 0.66, 1.0$ (outer-transparent, inner-transparent, inner-solid).

During the Ricci flow, the surface area ($A/(4\pi) = 0.999\,285$) is bound but not fixed through equation (27). The resulting round sphere metric $\mathrm{e}^{-2\sigma} q_{ij}$ has the total area of $A/(4\pi) = 1.007\,889$, which we normalize to unity. In the next step, we compute the $l = 1$ eigenfunctions n^j of this metric, as explained in section 3.3. As initial data for the relaxation method we picked $n^j|_{t=0} = \hat{n}^j$, where the parabolic flow was stable up to $\nu = 0.23$ for RK2. The three steady-state solutions are orthonormalized through the Gram–Schmidt process and inverted $n^j(\hat{n}) \to \hat{n}^j(n)$ using Newton–Raphson's method (since we have access to $\partial_i n^j$). In figure 3 (right), the old spherical coordinate lines $\hat{n}^j(n)$ are shown on the new grid on which we re-evaluate σ/the spherical round metric ${}^0q_{ij}$. The round metric in the canonical coordinates n^i can be embedded into Euclidean space by the shape function $h_0 = 1$. During the embedding flow, the shape is stepwise 'deformed' into the target shape function by solving the LEE at each step. Again the relaxation method with RK2 for $\nu = 0.2$ is employed.

We chose a conformal factor that is linear in t and then the change of $h_{(n)}$ during the first steps of the flow $n = 1, 2, 3$, $t_{n=0,1,2,3} = 0.0, 0.33, 0.66, 1.0$ is about linear in t as well which can be seen in figure 4 (left); the difference between consecutive shape functions is approximately constant along a fixed direction. The increase/decrease is strongest in the directions where the target metric differs the most from the round metric. This is also apparent in figure 4 (right) and figure 5, where the embeddings of $q(t, \sigma)_{ij}$ at different states of the flow are shown. The drifting of grid points as illustrated in figure 1 is not visualized but it can be seen how the unit sphere stepwise deforms into the target shape. The difference between $h_{(3)}$

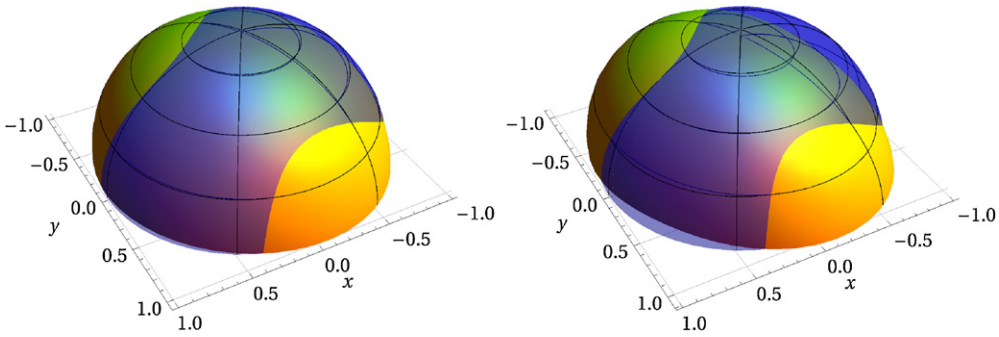

Figure 5. Embedding flow around unit sphere (transparent) at $t_1 = 0.33$ (left) and $t_3 = 1$ (right).

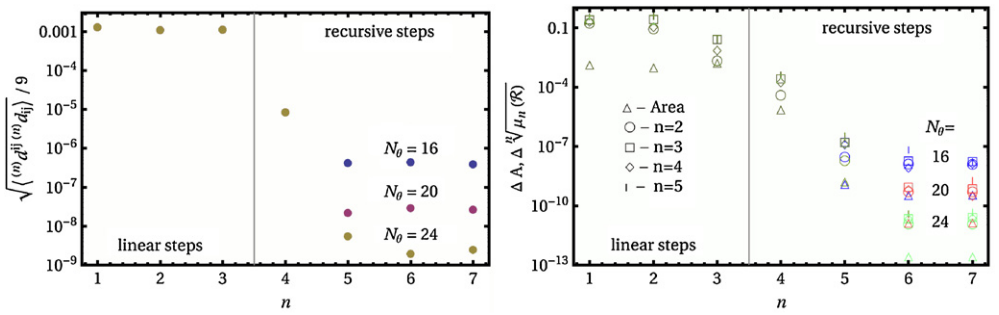

Figure 6. Left: difference between the flow and the induced metric at linear $t_{n=1,2,3} = 0.33, 0.66, 1$ and recursive iteration $t_{n=4-7} = 1$ of the embedding flow. Right: difference of the area A and $\mu_n(\mathcal{R})$ between the induced and target metric.

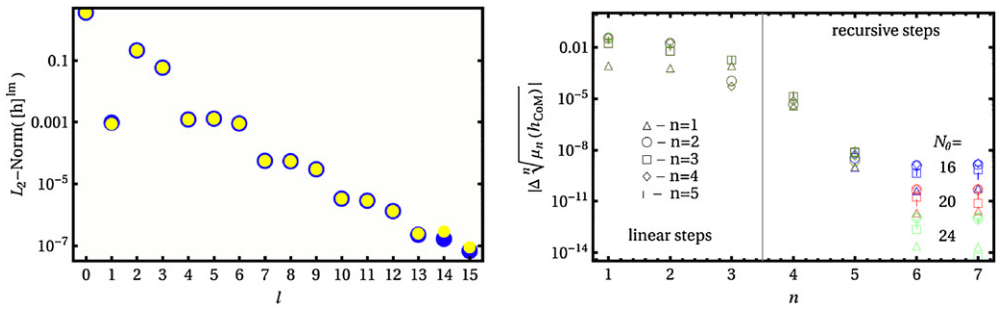

Figure 7. Left: L_2-norm: $\sqrt{\sum_{m=-l}^{l}([h]^{lm})^2}$ for the original shape function h and $h_{n=7}$ for $N_\theta = 16$. The numerical solution differs at high modes but also at $l = 1$ (circles do not overlap), since the L_2-norm is not translationally invariant. Right: the norm $\mu_n(h_{\mathrm{CoM}})$ on the other hand is invariant under translations, where h_{CoM} is the corresponding shape function shifted to its center of mass. Difference between the centered original and final shape functions μ_n converges with increasing resolution and flow time down to truncation error.

and the original shape function, see figure 6 (left), is about 10^{-2}; in order to refine the solution further, we recursively apply the LEE, whereby the difference between the target metric and induced metric d_{ij} as well as the intrinsic curvature converges exponentially with increasing n and increasing resolution, limited by a plateau of truncation error, see figure 6. Note that due to the non-uniqueness of the embedding, the final shape function is arbitrarily shifted and rotated w.r.t. to the original one. In figure 7 (left), the L_2-norm of the h function, decomposed

in spherical harmonics, is shown in each l-eigenspace. It is independent of rotations but not of translations, which is clearly visible in the different $l = 1$ modes. By shifting the shape functions to their center of mass $h \to h_{\mathrm{CoM}}$, we can compare the norms $\mu_n(h_{\mathrm{CoM}})$ which are invariant under both rotations and translations and show the same convergence behavior as before, see figure 7 (right).

5. Conclusion

In this paper, we presented a new numerical algorithm to solve the Weyl problem. The basic idea stems from the method of continuity which served as an approach in Nirenberg's proof of the existence and goes back to Weingarten and Weyl. The linearized embedding equations play a central role. They can be reduced to a single linear elliptic PDE by a transformation of variables. Solving the LEE stepwise for two 'nearby' metrics on a known embedding of one of the metrics allows one to 'slowly' deform an initial shape into the desired embedding (embedding flow). In doing so, it is necessary to link the target metric to an initial metric, whose embedding into $\mathbf{R}^3$ is known. For this purpose, the round metric is well suited which is a steady-state solution of the Ricci flow on S^2 that can be evolved from any metric. But it is then in general given in arbitrary coordinates.

Hence, apart from solving the embedding equations, a number of additional obstacles appear which complicate the numerical implementation of the method of continuity. Namely, we need to find a suitable coordinate system, solve various (non)-linear elliptic PDEs, (anti)-differentiate functions on the surface, handle the drifting of grid points under the embedding flow or the $SO(3, 1)$ freedom of the solution, etc. Another challenge is to keep the total numerical error of all steps small.

Through the use of over-determined quasi-Cartesian coordinates on the surface as well as spectral methods and the parabolic flow relaxation method, we have shown how to overcome these technical difficulties altogether without losing numerical accuracy. Note that the compatibility with the simulations in $(3 + 1)$ numerical relativity is automatically given, since our approach requires as input an arbitrary shape function as well as a Riemannian 3-manifold, both of which generate an admissible 2-metric on the surface. This allows direct applications in binary black hole simulations to measure quasi-local mass or to investigate the large-scale dynamics of numerical simulations of inhomogeneous cosmological models, where the coarse-graining process involves solving the isometric embedding problem. These quasi-local mass definitions, like the Brown–York or the Kijowski–Liu–Yau mass [6–9], are based on the comparison principle: anchor the intrinsic geometries by isometric embeddings and compare the extrinsic geometries. Moreover, isometric embeddings are ideal for visualizing 2-metrics because they are fixed by unique shapes in the Euclidean space.

We have implemented our method with Fortran90 and tested it on a concrete arbitrarily chosen initial shape function in the Euclidean space. By direct comparison between the final and initial shape functions and metrics, we were able to demonstrate exponential convergence by increasing the spherical resolution as well as the number of recursive iteration steps of the embedding flow. Our method is limited to positively curved and positive-definite 2-metrics and to ones whose isometric embedding and shape function in $\mathbf{R}^3$ are 'well represented' through harmonic polynomials within $l_{\mathrm{max}} < 40$, i.e. whose spherical harmonics power spectrum drops quickly enough, but is then guaranteed to reach a solution at reasonable computational cost, a few minutes on a modern CPU.

Apart from the applications already mentioned, the numerical methods in the sub-steps of our approach, like the implementation to solve the Ricci flow or the $l = 1$ EV problem, could lead to other applications in numerical relativity on their own, for example, to solve other

elliptic PDEs that appear to find approximate Killing vector fields on trapping horizons [20] or to correct the gravitational wave signal of binary black hole simulations that is commonly extracted on coordinate spheres at finite radius. In general, the spherical coordinates are distorted w.r.t. the $l = 1$ eigenfunctions of these spheres. Furthermore, there are quasi-local mass and momentum measures, see [21] and references therein, which require isometric embeddings into Minkowski space (and into $\mathbf{R}^3$ as a sub-step) that would allow one to measure the linear momentum in numerical BBH simulation quasi-locally.

Acknowledgements

MK would like to thank Lars Andersson and Luciano Rezzola for their invitation to the Max Planck Institute for Gravitational Physics in Potsdam, which has enabled us to continue collaborating on this project. MJ thanks Badri Krishnan, Alex Nielsen, Frank Ohme and Joachim Frieben for helpful comments and discussions. This work was supported by the IMPRS for Gravitational Wave Astronomy in the Max Planck Society.

Appendix A. Adjusting the spectrum of $\mathcal{L}$

In the case of a round sphere, the linear operator $\mathcal{L}$ is given by $-\Delta - 2$ which has only one negative eigenvalue $\lambda_0 = -2$. This property of the spectrum turned out to be true for all covex surfaces we were dealing with. Note that in order to apply the parabolic relaxation flow method, we require all eigenvalues to be either non-positive or non-negative. This can be achieved by modifying $\mathcal{L}$ in the following way.

First we define a new self-adjoint operator $\widetilde{\mathcal{L}}$ as

$$\widetilde{\mathcal{L}}(w) = \frac{1}{\sqrt{\mathcal{K}}}\,\mathcal{L}\left(\frac{w}{\sqrt{\mathcal{K}}}\right), \tag{A.1}$$

for which $\widetilde{\mathcal{L}}(\sqrt{\mathcal{K}}) = -\sqrt{\mathcal{K}}$; thus, its principal eigenvalue $\widetilde{\lambda}_0$ is -1. Now we modify $\widetilde{\mathcal{L}}$ to shift this eigenvalue to the positive part of the spectrum. This is straightforward given the fact that both the eigenvalue and the eigenfunction are explicitly known. We define a new operator

$$\widehat{\mathcal{L}}(w) = \widetilde{\mathcal{L}}(w) - \frac{C}{\langle\sqrt{\mathcal{K}}, \sqrt{\mathcal{K}}\rangle}\langle\sqrt{\mathcal{K}}, \widetilde{\mathcal{L}}(w)\rangle\,\sqrt{\mathcal{K}} \tag{A.2}$$

for a constant $C > 1$. $\widehat{\mathcal{L}}$ has a non-negative spectrum and can be used to solve (17) by the relaxation method. After simplification, the resulting parabolic equation reads

$$\dot{w} = -\frac{1}{\mathcal{K}}\,(\mathcal{L}(w) - \tau) + E\langle\mathcal{L}(w) - \tau\rangle, \tag{A.3}$$

where E is a sufficiently large, positive number.

Appendix B. Anti-differentiating a function

In section 2.3, we show that the vector field Y^i can be reconstructed from its derivatives on the sphere. This leads us to the following numerical problem: Given the gradient of a function on S^2 expanded in terms of spherical harmonics, what is the spherical harmonics decomposition of the original function?

Let f be a function expanded in terms of Y^{lm},

$$f = \sum_{l=0}^{+\infty}\sum_{m=-l}^{m=l} {}^{Y}[f]^{lm}\,Y^{lm}. \tag{B.1}$$

The ϕ derivative is

$$f_{,\phi} = \sum_{l=0}^{+\infty} \sum_{m=-l}^{m=l} {}^{Y}[f]^{lm}\, \mathrm{i}m\, Y^{lm}, \tag{B.2}$$

so for all coefficients with $m \neq 0$, we obtain a straightforward relation between the expansions of f and $f_{,\phi}$:

$${}^{Y}[f]^{lm} = -\frac{\mathrm{i}}{m}\, {}^{Y}[f_{,\phi}]^{lm}. \tag{B.3}$$

In general, the θ derivative of a regular f has a discontinuity at $\theta = 0, \pi$. This can be cured by multiplying it by $\sin\theta$. It is easy to see that $\sin\theta \frac{\partial}{\partial\theta} Y^{l,m}$ can be expressed in terms of other spherical harmonics with the same m. In particular, the harmonics with $m = 0$ satisfy

$$\sin\theta \frac{\partial}{\partial\theta} Y^{l,0} = \frac{l(l+1)}{\sqrt{(2l+1)(2l+3)}}\, Y^{l+1,0} + \frac{l(l+1)}{\sqrt{(2l-1)(2l+1)}}\, Y^{l-1,0}. \tag{B.4}$$

This equation gives us a recurrence relation for the $m = 0$ coefficients of f in terms of $\sin\theta \frac{\partial f}{\partial\theta}$,

$${}^{Y}[f]^{l,0} = -\frac{\sqrt{(2l-1)(2l+1)}}{l(l+1)}\, {}^{Y}[\sin\theta f_{,\theta}]^{l-1,0} + \frac{(l-1)(l-2)}{l(l+1)} \sqrt{\frac{2l+1}{2l-3}}\, {}^{Y}[\sin\theta f_{,\theta}]^{l-2,0} \tag{B.5}$$

valid for $l \geqslant 2$. For $l = 1$, the relation reads

$${}^{Y}[f]^{1,0} = -\frac{\sqrt{3}}{2}\, {}^{Y}[\sin\theta f_{,\theta}]^{0,0}. \tag{B.6}$$

Finally, the ${}^{Y}[f]^{0,0}$ coefficient is arbitrary. This corresponds to the possibility of adding a constant to the solution.

References

[1] Han Q and Hong J X 2006 *Isometric Embedding of Riemannian Manifolds in Euclidean Spaces* (Povidence, RI: American Mathematical Society)
[2] Spivak M 1979 *A Comprehensive Introduction to Differential Geometry* vol 5 (Berkeley, CA: Publish or Perish)
[3] Alexandrov A D 1941 *Dokl. Akad. Nauk SSSR* **50** 103–6
[4] Pogorelov A V 1949 *Usp. Mat. Nauk* **32** 183–6
[5] Nirenberg L 1953 *Commun. Pure Appl. Math.* **6** 337–94
[6] Kijowski J 1997 *Gen. Rel. Grav.* **29** 307
[7] Brown J and York James W J 1991 *Mathematical Aspects of Classical Field Theory* ed M J Gotay, J E Marsden and V Moncrief (Providence, RI: American Mathematical Society) pp 129–42
[8] Brown J and York James W J 1993 *Phys. Rev.* D **47** 1407–19 (arXiv:gr-qc/9209012)
[9] Liu C C M and Yau S T 2003 *Phys. Rev. Lett.* **90** 231102 (arXiv:gr-qc/0303019)
[10] Szabados L B 2004 *Living Rev. Relativ.* **7** 10 (www.livingreviews.org/lrr-2004-4)
[11] Korzyński M 2010 *Class. Quantum Grav.* **27** 105015 (arXiv:0908.4593)
[12] Korzyński M 2010 *AIP Conf. Proc.* **1241** 973–80 (arXiv:1001.2031)
[13] Nollert H P and Herold H 1996 Visualization in curved spacetimes: II. Visualization of surfaces via embeddings *Relativity and Scientific Computing* (Berlin: Springer) pp 330–51
[14] Bondarescu M, Alcubierre M and Seidel E 2002 *Class. Quantum Grav.* **19** 375
[15] Hamilton R 1988 *Math. Gen. Relativ. Contemp. Math.* **71** 237–61
[16] Chow B 1991 *J. Differ. Geom.* **33** 325–34
[17] Cao H D, Chow B, Chu S C and Yau S T (ed) 2003 *Collected Papers on Ricci Flow (International Press Series in Geometry and Topology* vol 37*)* (Sommerville, MA: International)
[18] Weingarten J 1886 *Crelle's J.* **100** 296–310
[19] Jasiulek M 2009 *Class. Quantum Grav.* **26** 245008 (arXiv:0906.1228)
[20] Cook G B and Whiting B F 2007 *Phys. Rev.* D **76** 041501 (arXiv:0706.0199)
[21] Wang M T and Yau S T 2009 *Commun. Math. Phys.* **288** 919–42 (arXiv:0805.1370)